Tellurium isotope cosmochemistry: Implications for volatile fractionation in chondrite parent bodies and origin of the late veneer

Jan L. Hellmann[a,*], Timo Hopp[a,b], Christoph Burkhardt[a], Harry Becker[c], Mario Fischer-Gödde[a,d] and Thorsten Kleine[a]

[a] *Institut für Planetologie, Westfälische Wilhelms-Universität Münster, Wilhelm-Klemm-Straße 10, 48149 Münster, Germany*

[b] *Origins Laboratory, Department of the Geophysical Sciences and Enrico Fermi Institute, The University of Chicago, 5734 South Ellis Avenue, Chicago, IL 60637, USA*

[c] *Institut für Geologische Wissenschaften, Freie Universität Berlin, Malteserstraße 74-100, 12249 Berlin, Germany*

[d] *Institut für Geologie und Mineralogie, Universität zu Köln, Zülpicher Straße 49b, 50674 Köln, Germany*

[*]Corresponding author at: Institut für Planetologie, Westfälische Wilhelms-Universität Münster, Wilhelm-Klemm-Straße 10, 48149 Münster, Germany.

E-mail address: jan.hellmann@uni-muenster.de (J. L. Hellmann).

Abstract

Tellurium stable isotope compositions and abundances ($\delta^{128/126}$Te relative to SRM 3156) are reported for 43 ordinary, enstatite, and Rumuruti chondrites, which together with results from a companion study on carbonaceous chondrites are used to assess the origin of volatile element fractionations in chondrites. Whereas Te isotope variations among carbonaceous chondrites predominantly reflect mixing between isotopically light chondrules/chondrule precursors and CI-like matrix, Te isotope variations among non-carbonaceous chondrites mainly result from Te redistribution during parent body thermal metamorphism. The enstatite chondrites in particular display increasingly heavy Te isotopic compositions and decreasing Te concentrations with increasing degree of metamorphism, indicating migration of isotopically light Te from the strongly metamorphosed inner parts towards the cooler outer regions of the parent bodies. By contrast, ordinary and Rumuruti chondrites display less systematic Te isotope variations, implying more localized redistribution of Te during parent body thermal metamorphism.

We also report Te stable isotope data for 19 terrestrial mantle-derived rocks. Peridotites with Al_2O_3 contents close to those inferred for the bulk silicate Earth (BSE) exhibit uniform $\delta^{128/126}$Te values, which we interpret to represent the Te isotopic composition of the BSE. This composition overlaps with the Te isotope composition of some volatile-rich carbonaceous chondrites (most notably CM chondrites), but also with that of enstatite chondrites. Comparison of the Te results to Se isotopes and Se/Te ratios shows that due to uncertainties in the composition of the BSE and the isotopic composition of bulk chondrite parent bodies, neither Te isotopes alone nor the combined Se-Te elemental and isotopic systematics can distinguish between a carbonaceous and enstatite chondrite-like late veneer, which is the presumed source of Se and Te in the BSE. Together, the results of this study illustrate that the relative abundances and mass-dependent isotope compositions of volatile elements like Se and Te are modified by physical and chemical processes occurring after planetary accretion, which severely complicates their use as genetic tracers. A corollary of this is that contrary to prior proposals the Se-Te systematics are not contradicting an inner solar system origin of the late veneer, as it has been inferred using nucleosynthetic isotope anomalies of other elements.

Keywords

Tellurium; Te isotopes; Mass-dependent isotope fractionation; Ordinary chondrites; Enstatite chondrites; Rayleigh fractionation; Thermal metamorphism; Late accretion; Bulk silicate Earth; Peridotites

1 Introduction

Late accretion is defined as the continued addition of material to Earth's mantle after the cessation of core segregation (e.g., Walker, 2009). Understanding the nature and composition of the late-accreted material (commonly termed the 'late veneer') and whether it derives from the inner or outer solar system is of considerable interest. For instance, a volatile-rich late veneer from the outer solar system may have been the dominant source of Earth's water and highly volatile elements (e.g., Varas-Reus et al., 2019; Wang and Becker, 2013). However, from a dynamical standpoint it seems more likely that the late veneer derives from left-over planetesimals from the terrestrial planet region with only little contribution from outer solar system planetesimals (e.g., Jacobson et al., 2014). Thus, determining the genetic heritage and composition of the late veneer may help assessing the origin and timing of the delivery of Earth's water and highly volatile elements, and the compositional spectrum and heritage of planetesimals bombarding the terrestrial planets after the Moon-forming impact.

The primary evidence for late accretion comes from the highly siderophile element (HSE) abundances inferred for the bulk silicate Earth (BSE), which are higher than expected for metal-silicate equilibration during core formation (e.g., Chou, 1978; Kimura et al., 1974; Mann et al., 2012), but are consistent with the addition of ~0.5 wt.% of broadly chondritic material to Earth's mantle (Becker et al., 2006; Day et al., 2017; Kimura et al., 1974; Walker, 2009). Accordingly, the composition and genetic heritage of the late-accreted material have mainly been studied using the elemental abundances and isotopic compositions of the HSE. For instance, the $^{187}Os/^{188}Os$ ratio of the BSE (reflecting its time-integrated Re/Os) overlaps with enstatite and ordinary chondrites, but is distinct from most carbonaceous chondrites (Meisel et al., 1996; Meisel et al., 2001). The BSE's $^{187}Os/^{188}Os$ may be consistent with the contribution of carbonaceous chondrites to late accretion if the late veneer also contained a fractionated metal component with elevated Re/Os (Fischer-Gödde and Becker, 2012), but it was later shown that this was likely not the case (Hopp and Kleine, 2018). Consequently, the Os isotopic composition of the BSE is best explained by an enstatite or ordinary chondrite-like late veneer (e.g., Walker et al., 2015). Consistent with this, nucleosynthetic Ru isotope anomalies also support an enstatite chondrite-like late veneer, because the BSE's Ru isotopic composition is most similar to those of enstatite chondrites, whereas all other chondrites, and in particular carbonaceous chondrites and iron meteorites, are characterized by a deficit in *s*-process Ru isotopes and, therefore, are unlikely sources of the late veneer (Bermingham and Walker, 2017; Bermingham et al., 2018; Dauphas et al., 2004; Fischer-Gödde et al., 2015; Fischer-Gödde and Kleine, 2017; Hopp et al., 2020; Worsham et al., 2019). More recently, it has been proposed that not all the BSE's Ru derived from late accretion, and that the BSE's Ru isotopic composition reflects a mixture between pre-late veneer Ru characterized by an excess in *s*-process Ru with late accretion-derived Ru characterized by an *s*-process deficit (Fischer-Gödde et al., 2020). This model would allow for the contribution of carbonaceous chondrite-like material to late accretion, but does not require it, because most non-carbonaceous meteorites are also characterized by variable *s*-process deficits for Ru (e.g., Bermingham et al., 2018; Fischer-Gödde et al., 2015; Hopp et al., 2020).

The genetic heritage and composition of the late veneer has also been studied using the chalcophile (to highly siderophile) volatile elements Se, Te, and S. As for the HSE, it is commonly assumed that S, Se, and Te in the BSE predominantly derived from late accretion (Palme and O'Neill, 2014; Wang and Becker, 2013). Wang and Becker (2013) observed that the ratios of S, Se, and Te inferred for the BSE from terrestrial mantle peridotites are distinct from enstatite chondrites, but overlap with volatile-rich carbonaceous

chondrites and most notably CM chondrites. On this basis, these authors argued for a CM-like source of the late veneer. Along similar lines, Varas-Reus et al. (2019) showed that the mass-dependent Se isotope composition of peridotites overlaps only with CI chondrites, and so these authors suggested a CI-like late veneer. However, other studies have argued that for elements like Se and Te, peridotites do not provide reliable proxies for the composition of the BSE and that, therefore, these data do not allow constraining late accretion (e.g., König et al., 2014; Yierpan et al., 2019). Moreover, not all the BSE's S (and by implication perhaps also Se and Te) may derive from late accretion (Labidi et al., 2013; Suer et al., 2017), which further complicates the application of these elements as tracers of late accretion.

To further add to this debate, we obtained mass-dependent Te isotopic data for a large set of terrestrial mantle rocks and chondrites. Although a previous Te isotopic study argued for a carbonaceous chondrite-like source of the late veneer (Fehr et al., 2018), that study did not report resolved Te isotopic differences between the different classes and groups of chondrites. Moreover, thermal metamorphism on chondrite parent bodies may have resulted in volatilization, redistribution, and isotopic fractionation of volatile elements (e.g., Wombacher et al., 2003), but to what extent this affected the Te isotopic composition of enstatite and ordinary chondrites is unknown. This information is crucial, however, because utilizing Te isotopes as a genetic tracer of the late veneer requires knowledge of the representative composition of bulk chondrite parent bodies. Finally, a precise estimate of the BSE's Te isotopic composition is lacking, because until now only terrestrial sedimentary rocks and solution standards were analyzed. To overcome these limitations, we obtained Te isotopic data for several ultramafic terrestrial mantle rocks and a comprehensive set of chondrites from all major groups. These data are used to examine the effect of thermal metamorphism on Te isotope compositions and abundances in chondrites, to estimate the Te isotopic composition of the BSE, and to assess the feasibility of Se, Te, and S to constrain late accretionary sources. As such, this study may help resolve the inconsistencies between late veneer sources inferred from HSE and S-Se-Te systematics.

2 Samples and analytical methods

2.1 Samples

Forty-three bulk chondrites were selected for this study, including 20 ordinary (H, L, LL chondrites of petrologic type 3–6), 21 enstatite (EH3-5, EL3-6), and two Rumuruti chondrites (R3.8-3.9). Tellurium isotopic data for a comprehensive set of carbonaceous chondrites are reported in a companion study, which used the same analytical setup as this study (Hellmann et al., 2020). In addition, 19 ultramafic terrestrial mantle rocks were analyzed, comprising 13 massif-type peridotites from different geological setting and six pyroxenites from the Balmuccia (BM) peridotite massif. The peridotites comprise ten lherzolites (2.1–3.9 wt.% Al_2O_3), two harzburgites (1.1–1.8 wt.% Al_2O_3), and one dunite (0.3 wt.% Al_2O_3), whereas the pyroxenites include two spinel clinopyroxenites, one orthopyroxenite, and two websterites. Most of the terrestrial samples are well characterized for their major and trace element compositions, including abundances of S, Se, and Te as well as the HSE, and were described as fresh and unaltered (Fischer-Gödde et al., 2011; Wang and Becker, 2013, 2015b; Wang et al., 2013). These samples were previously used to estimate the Se/Te ratio of the BSE (Wang and Becker, 2013).

2.2 Analytical Methods

Sample powders of bulk chondrites (~50-450 mg, from >2 g bulk powders), peridotites (~2-3 g aliquots from ~100 g bulk powders) and pyroxenites (~0.5-2 g aliquots from ~0.5-5 g bulk powders) were weighed into 60 ml (chondrites) or 90 ml (peridotites and pyroxenites) Savillex PFA vials and mixed with appropriate amounts of ^{123}Te-^{125}Te double spike (Hellmann et al., 2020). The spiked samples were dissolved in 2:1 HF–HNO_3 on a hot plate for 2-3 days at 120-150 °C. After dissolution, samples were evaporated to dryness at 120 °C and the residues were taken up and dried several times in concentrated HNO_3 to destroy fluorides that may have formed during digestion. The samples were then converted to chloride form by several dry downs in concentrated HCl, and re-dissolved in 25 mL 2 M HCl for ion exchange chemistry.

Tellurium was separated from the sample matrix using a three-stage column chromatography described in Hellmann et al. (2020). In brief, samples were loaded in 25 mL 2 M HCl onto pre-cleaned anion exchange columns filled with 5 mL BioRad AG1X8 resin (200-400 mesh). After sequential washes of 15 mL 2 M HCl, 7 mL 11 M HCl, and 15 mL 5 M HF, Te was eluted in 10 mL 1 M HNO_3. Organic compounds in the Te fractions were removed by dry-downs in concentrated HNO_3. Following conversion to chloride form, samples were dissolved in 1 mL 2 M HCl and loaded onto a clean-up column filled with 1 mL pre-cleaned BioRad AG1X8 resin (200-400 mesh). After sequential washes with 5 mL 2 M HCl, 2 mL 11 M HCl, and 5 mL 5 M HF, Te was eluted using 6 mL 0.5 M HCl. The third chemistry was performed to separate Mo from Te and was only applied to chondrites (as peridotites and pyroxenites have much lower Mo/Te ratios). The Te fractions of chondrite samples from the second chemistry were evaporated to dryness several times in HNO_3 and then dissolved in 1 mL 7 M HNO_3. The sample solutions were loaded onto pre-cleaned columns (500 µl TRU resin-B, 50-100 µm) and Te was directly collected together with an additional elution of 4 mL 7 M HNO_3. All samples were repeatedly dried down in HCl–HNO_3 and HNO_3, and the final Te fractions were dissolved in 0.28 M HNO_3 for isotope measurements.

All Te isotope measurements were performed using a ThermoScientific Neptune *Plus* multi-collector ICP-MS at the Institut für Planetologie and followed the measurement routine described in Hellmann et al. (2020). Samples were introduced using a Cetac Aridus II desolvator and a Savillex C-flow nebulizer at an uptake rate of ~40 µl/min. Sample solutions were measured at ~100 ng ml^{-1} Te (chondrites) or at ~30-50 ng ml^{-1} Te (peridotites and pyroxenites) using standard sampler and X skimmer cones. For a 100 ng ml^{-1} standard solution this configuration yielded total ion beam intensities of ~2–2.5 x 10^{-10} A. Ion beams were collected simultaneously using Faraday cups connected to 10^{11} Ω feedback resistors for ^{123}Te, ^{125}Te, ^{126}Te, and ^{128}Te, and Faraday cups connected to 10^{12} Ω feedback resistors for ^{121}Sb and ^{129}Xe. Prior to each analysis the sample introduction system was washed using 0.28 M HNO_3 for 10-15 min. Each measurement consisted of on-peak background measurements of 100 x 1.05 s integrations, followed by sample measurements of 50 cycles of 4.2 s each. Constant isobaric interferences of Xe on ^{126}Te and ^{128}Te from the Ar gas were corrected using on-peak background measurements. Interferences of residual Sb (on ^{123}Te) and Xe were corrected iteratively using the exponential mass fractionation law, but were insignificant for all samples.

The measured raw data were processed off-line following the three-dimensional data reduction routine of Siebert et al. (2001), using ^{123}Te/^{128}Te, ^{125}Te/^{128}Te and ^{126}Te/^{128}Te ratios. The double spike inversion provides the natural fractionation factor α, for which the Te stable isotopic composition of a sample is calculated as follows:

$$\delta^{128/126}\mathrm{Te}_{\mathrm{sample}} = -1000 \times \left(\alpha_{\mathrm{sample}} - \alpha_{\mathrm{Mean\ NIST\ SRM\ 3156}}\right) \times \ln(m_{128}/m_{126}) \quad (1)$$

where m_{128} and m_{126} are the atomic weights of ^{128}Te and ^{126}Te and $\alpha_{\mathrm{Mean\ NIST\ SRM\ 3156}}$ is the mean natural fractionation factor α of a spiked bracketing NIST SRM 3156 standard solution measured at similar concentrations in the same measurement sequence. Here $\delta^{128/126}$Te is defined as the permil deviation of the ^{128}Te/^{126}Te ratio of a sample from the composition of the NIST SRM 3156 Te standard:

$$\delta^{128/126}\mathrm{Te} = \left[\frac{\left(^{128}\mathrm{Te}/^{126}\mathrm{Te}\right)_{\mathrm{sample}}}{\left(^{128}\mathrm{Te}/^{126}\mathrm{Te}\right)_{\mathrm{SRM3156}}} - 1\right] \times 1000 \quad (2)$$

The results for samples are reported as the mean of replicate measurements (n = 3–8) with their corresponding two standard deviation (2s.d.). Due to their low Te abundances, dunite BM11-07A and pyroxenite BM-11-26 could only be measured once at ~30 ng ml^{-1}, and the uncertainty of these measurements (±0.02) were estimated by averaging the 2s.d. obtained for the other terrestrial samples measured at ~30 ng ml^{-1}.

3 Results

3.1 Chondrites

The Te concentrations and stable isotope compositions of ordinary, enstatite, and Rumuruti chondrites are provided in Table 1 and shown in Fig. 1 together with previously published Te isotopic data for carbonaceous chondrites (Hellmann et al., 2020). The non-carbonaceous chondrites of this study exhibit an overall range of ~1‰ amu^{-1}, and Te concentrations vary between ~140 and ~2700 ng g^{-1}. By contrast to most carbonaceous chondrites, the enstatite, ordinary, and Rumuruti chondrites display substantial within-group $\delta^{128/126}$Te variations, and several type 5 and 6 enstatite and ordinary chondrites exhibit much heavier Te isotopic compositions than type 3 and 4 samples (Fig. 1).

Among the enstatite chondrites, the type 3-4 samples of both the EH (except Sahara 97072) and EL groups have indistinguishable $\delta^{128/126}$Te averaging at 0.01±0.06 (2 s.d., n = 11), and homogeneous Te concentrations of ~2 µg g^{-1} and ~1.4–1.5 µg g^{-1}, respectively (Fig. 2a). The higher Te concentration of EH compared to EL chondrites probably reflects the higher metal content of the former, but evidently did not result in a resolvable Te isotopic difference between the two groups. Sahara 97072 is the only type 3 enstatite chondrite with a heavier Te isotopic composition, but its Te concentrations is similar to those of other EH3-4 chondrites. By contrast, type 5-6 enstatite chondrites display heavier, more variable Te isotope compositions and lower Te concentrations. Together, the enstatite chondrites reveal a broad trend towards lower Te concentrations and heavier isotopic composition with increasing petrologic type (Fig. 2a).

The ordinary chondrites of this study display a similar range in $\delta^{128/126}$Te as the enstatite chondrites, but overall exhibit less systematic behavior (Fig. 2b). Although some type 5-6 samples have very high $\delta^{128/126}$Te (Kunashak, Knyahinya, Ramsdorf), the ordinary chondrites display only a weak trend between $\delta^{128/126}$Te and Te concentration, and type 3-4 ordinary chondrites have variable $\delta^{128/126}$Te (Figs. 1, 2b). This

is consistent with results from Fehr et al. (2018), who reported large Te isotope variations among type 3 ordinary chondrites, and with the Te isotopic data for the two Rumuruti chondrites of this study, which display very different $\delta^{128/126}$Te, yet are both petrologic type 3 (Table 1 and Fig. 1).

3.2 Terrestrial samples

The Te concentrations and stable isotope compositions of terrestrial samples analyzed in this study are provided in Table 2 and Figs. 1 and 3. The 13 peridotites display rather homogeneous $\delta^{128/126}$Te, with values ranging from 0.00±0.01 (BM-11-11) to 0.11±0.01 (BB-3A and BD-92-2). The Te concentrations of these samples vary from ~3 to ~12 ng g^{-1}, but there is no obvious correlation between $\delta^{128/126}$Te and Te concentration (Fig. 3a). Importantly, lherzolites with Te concentrations between ~10 and ~12 ng g^{-1} display indistinguishable $\delta^{128/126}$Te values averaging at 0.09±0.03 (2s.d., n=9). These lherzolites also have the highest Al_2O_3 content and were previously interpreted to represent the Te concentration of the BSE (Wang and Becker, 2013).

The pyroxenites display variable $\delta^{128/126}$Te (–0.37 to 0.32) and Te concentrations (~2 to ~104 ng g^{-1}; Fig. 3b). The large $\delta^{128/126}$Te variation is almost entirely reflected by the three spinel clinopyroxenites, whereas the websterites and the orthopyroxenite show only small $\delta^{128/126}$Te variations from ~0.10 to 0.16. All pyroxenites, except for the spinel clinopyroxenite BM-11-15, have similar or heavier Te isotope compositions than the lherzolites.

4 Discussion

4.1 Comparison to previous studies

The comparison of the mass-dependent Te isotopic data of this study to those of a prior study on chondrites (Fehr et al., 2018) is somewhat complicated by the use of different standards in both studies. Whereas Fehr et al. (2018) reported their data relative to an in-house Te standard solution, this study reports the data relative to the NIST 3156 standard. Although Fehr et al. (2018) also measured the NIST 3156 standard, they used a different batch of this standard (Lot. No. 892901) than this study (Lot. No. 140830), which may be isotopically different (Hellmann et al., 2020).

To facilitate direct comparison between the data from both studies, we, therefore, analyzed the NIST 3156 and Alfa Aesar Te standard solutions used in Fehr et al. (2018). Both standard solutions are isotopically heavy compared to the NIST 3156 standard used in this study, with $\delta^{128/126}$Te values of 0.15±0.03 (NIST 3156, Lot. No. 892901) and 0.20±0.02 (Alfa Aesar metal). For a direct inter-study comparison, we, therefore, re-normalized the Te isotopic data from Fehr et al. (2018) for the offset between the two NIST 3156 batches used in the two studies. The comparison of the data from this study to the re-normalized data of Fehr et al. (2018) show a general good agreement for samples common to both studies, but also reveal a small systematic offset of about 0.02‰ amu^{-1} (Fig. S1). This small offset is similar to the analytical precision of Te isotopic data from both studies, and may reflect uncertainties introduced by the re-normalization to a common reference standard. We will, therefore, restrict the discussion of the Te isotopic data for chondrites to the data of this study and Hellmann et al. (2020), which both were obtained

using the same analytical methods and double spike, and together provide a comprehensive data set for 56 bulk chondrites from all major classes and groups.

4.2 Tellurium isotope fractionation and redistribution on chondrite parent bodies

Owing to its low condensation temperature (50% T_C ~700 K; Wood et al., 2019) and variable geochemical behavior under different redox conditions (e.g., Kadlag and Becker, 2017), Te is sensitive to elemental and isotopic fractionations by nebular and parent body processes. For instance, the Te isotopic variations among different groups of carbonaceous chondrites reflect variable mixtures of volatile-poor and isotopically light chondrules/chondrule precursors and volatile-rich and isotopically heavy CI-like matrix (Hellmann et al., 2020), indicating volatility-related Te isotopic fractionation during high-temperature processes in the solar nebula. Nevertheless, different samples of a given carbonaceous chondrite group display indistinguishable $\delta^{128/126}$Te and very similar Te concentrations, demonstrating that parent body processes (i.e., aqueous alteration and mild thermal metamorphism) had no significant effect on the Te elemental and isotope systematics of most carbonaceous chondrites (Hellmann et al., 2020). Tellurium isotope fractionations among carbonaceous chondrites thus predominantly reflect high-temperature processes in the solar nebula.

By contrast, the data of this study reveal that non-carbonaceous chondrites display substantial within-group Te isotopic heterogeneity, where type 5-6 samples tend to show more variable and heavier Te isotope compositions than type 3-4 samples of the same group. Similar systematics were previously observed for other volatile elements such as Zn (e.g., Luck et al., 2005; Moynier et al., 2011) and Cd (Wombacher et al., 2008; Wombacher et al., 2003), and have been interpreted to indicate mobilization and associated isotope fractionation of volatile elements during parent body metamorphism.

Below we will examine how the Te isotope fractionations among enstatite and ordinary chondrites fit into this model of volatilization and redistribution of volatile elements during parent body thermal metamorphism and will use this information to estimate the characteristic bulk $\delta^{128/126}$Te of their parent bodies. The latter is important for using $\delta^{128/126}$Te as a tracer for the origin of the late-accreted material added to Earth's mantle after cessation of core formation (sect. 4.4).

4.2.1 Enstatite chondrites

With the exception of one sample (Sahara 97072), the EH and EL chondrites of petrologic types 3-4 analyzed in this study have indistinguishable $\delta^{128/126}$Te, whereas all type 5 and 6 samples are isotopically heavier (by ~0.1-1.5‰) and exhibit lower Te concentrations than the type 3 and 4 samples of the same group (Fig. 2a). Similar systematic isotope variations have been observed for Zn (Moynier et al., 2011) and Cd (Wombacher et al., 2008), which also display heavy isotope compositions and lower element concentrations in type 6 enstatite chondrites. The volatile depletion of type 5-6 enstatite chondrites extends to several other volatile elements (e.g., Se, Ag, In, Bi, Tl) and, therefore, appears to be a characteristic feature of strongly metamorphosed enstatite chondrites (Ikramuddin et al., 1976; Wang and Lipschutz, 2005). Thus, the observed systematic Te isotope variations are most likely linked to the processes that governed the redistribution of volatile elements among enstatite chondrites.

Shock metamorphism may have led to mobilization and redistribution of volatile elements (e.g., Friedrich et al., 2004), but strongly shocked EL3-4 samples (shock stage S3 or S4) display less fractionated Te isotopic compositions than some EL5-6 samples with lower shock stage S2 (Fig. 4c,d). Furthermore, the most strongly shocked sample of this study (PCA 91020, S5) has the same $\delta^{128/126}$Te as other, less shocked type 3-4 enstatite chondrites. Thus, shock metamorphism does not seem to have had a significant effect on the Te isotope composition of enstatite chondrites. Instead, the systematically heavier Te isotope composition and stronger Te depletion in type 5-6 compared to type 3-4 enstatite chondrites indicates that volatilization and redistribution of Te occurred during parent body thermal metamorphism (Figs. 2a and 4a,b). This is consistent with heating experiments on the EH4 chondrite Abee, which reveal systematic loss of volatiles, and in particular Te, with increasing temperature (Ikramuddin et al., 1976).

The redistribution of volatile elements during thermal metamorphism can be envisioned with a thermally stratified structure of the parent body, in which volatile elements in the hotter inner parts were volatilized and migrated towards the cooler outer regions where they may have partially re-condensed. Such processes are capable of producing isotope fractionations, mainly because lighter isotopes enter the gas phase more readily and are, therefore, preferentially mobilized (e.g.,Wombacher et al., 2008). As such, these processes are expected to result in volatile-depleted and isotopically heavy compositions in the more strongly heated interior parts of a parent body. This is consistent with the systematically heavier Te isotopic composition of type 5-6 compared to type 3-4 enstatite chondrites. However, the decrease in Te concentrations among type 5-6 samples is not accompanied by a monotonous increase in $\delta^{128/126}$Te values, but instead led to a considerable range of heavy Te isotope compositions relative to type 3-4 samples (Fig. 2a). Moreover, the magnitude of the observed Te isotope variations is less than ~20% of those expected for kinetic Rayleigh evaporation (Fig. 5), consistent with prior observations for Cd isotope variations in enstatite and ordinary chondrites (Wombacher et al., 2008). Together, this indicates a more complex evaporation and condensation history than simple partial kinetic Rayleigh evaporation, where the overall magnitude of isotope fractionation was likely suppressed due to back-reaction and recondensation of volatilized Te during vapor transport through the parent body. Additionally, diffusion of Te during thermal metamorphism can produce isotopic heterogeneity on the sample scale because lighter isotopes diffuse faster relative to heavier isotopes leading to heterogeneous distribution of isotopically fractionated Te. This interpretation is similar to a model developed in a prior study based on Cd isotope variations in ordinary chondrites (Wombacher et al., 2008).

The upward migration of isotopically light volatile elements to the cooler, outer parts of the parent body may result in depletions or enrichments of volatile elements, as well as light and heavy isotopic compositions, depending on whether the vapor re-condensed or was lost from the system. Such open-system thermal metamorphism is consistent with the elemental and isotope variations observed for Cd (Wombacher et al., 2003) and Te (Fehr et al., 2018; this study) among type 3 ordinary chondrites (see below). Wang and Lipschutz (2005) proposed that this process can also account for the variable volatile element abundances of enstatite chondrites. However, the data of this study reveal that type 3-4 enstatite chondrites have rather homogeneous Te isotope compositions and fairly constant within-group Te concentrations. This suggests that the mobilized, isotopically light Te from deeper regions of the parent body was homogeneously distributed throughout the upper regions from where the type 3-4 samples derive. However, such homogenization is unexpected if the mobilized and isotopically light Te migrated through the porous upper layers of a parent body and was lost to space, which should have rather led to Te isotope variations as observed for type 3 ordinary chondrites. Thus, the homogeneous Te isotope compositions of

type 3-4 enstatite chondrites suggest efficient sealing of possible pathways for volatile loss, perhaps through impact heating or sintering during the lower-grade thermal metamorphism of type 3-4 samples.

Alternatively, type 3-4 samples derive from a distinct parent body than type 5-6 samples and in this case may have never received isotopically fractionated Te from underlying, hotter regions of the parent body. Either way, the variable Te concentrations and isotope compositions of enstatite chondrites make it difficult to estimate a representative bulk $\delta^{128/126}$Te for their parent bodies. Through the redistribution of isotopically light Te within the parent bodies, it seems unlikely that enstatite chondrites of any petrologic type retained their original Te isotopic composition (except perhaps type 3-4 samples, if they derive from different parent bodies than type 5-6 samples). Instead, the $\delta^{128/126}$Te of bulk enstatite chondrite parent bodies was likely lighter than the composition measured for type 5-6 samples, but heavier than the composition measured for type 3-4 samples. The latter contain much more Te than the former, and so the bulk parent body $\delta^{128/126}$Te will likely be closer to the $\delta^{128/126}$Te value of type 3-4 samples. We will return to this issue below when using $\delta^{128/126}$Te to assess the nature of the late veneer (sect. 4.4).

4.2.2 Ordinary chondrites

The ordinary chondrites of this study display a similar extent of Te isotope variations as the enstatite chondrites, but the range of Te concentrations is much smaller (Fig. 2). Moreover, while most type 5-6 enstatite chondrites have $\delta^{128/126}$Te values >0.4, most type 5-6 ordinary chondrites display smaller $\delta^{128/126}$Te, and only three samples have heavier compositions (Ramsdorf, Knyahinya, Kunashak). Of these, Ramsdorf probably is an impact melt rock (Yamaguchi et al., 1999), and so its heavy Te isotope composition may reflect impact-induced melting and volatilization. Overall, there is no obvious systematic variation of $\delta^{128/126}$Te with ordinary chondrite group or petrologic type (Fig. 6). Thus, neither the different metal contents or redox compositions of H, L, and LL chondrites, nor the different degree of thermal metamorphism resulted in systematic Te isotopic variations. Moreover, $\delta^{128/126}$Te values are not correlated with Te concentrations, and ordinary chondrites of all sub-groups and petrologic types rather cluster between ~250 and 450 ng g^{-1} Te independent of $\delta^{128/126}$Te. Thus, in contrast to enstatite chondrites, Te isotope variations among ordinary chondrites are less systematic and show no stringent relation between Te mobilization and isotopic fractionation with the degree of metamorphism.

A similar unsystematic behavior has previously been observed for Cd isotopes in ordinary chondrites, although the overall range of Cd isotope variations seems to be somewhat larger: the $\delta^{114/110}$Cd of ordinary chondrites vary by ~20 ‰ (Wombacher et al., 2008), whereas $\delta^{128/126}$Te varies by only ~6 ‰ (including data for type 3 ordinary chondrites from Fehr et al., 2018). This difference likely reflects the approximately two times larger relative mass difference of ^{114}Cd/^{110}Cd compared to ^{128}Te/^{126}Te, and the lower condensation temperature/higher mobility of Cd compared to Te (Schaefer and Fegley, 2010). Thus, the Te and Cd isotope variations among ordinary chondrite were likely set by the same processes. Wombacher et al. (2008) proposed that the Cd isotope variations reflect volatilization and redistribution of gaseous Cd during parent body metamorphism, that is, a similar process as described above for Te isotope variations in enstatite chondrites. However, unlike for the enstatite chondrites, there is no evidence for systematic redistribution of Te from the inner more strongly metamorphosed parts (as sampled by type 5-6 chondrites) to the upper, less strongly heated shells of the parent body from where type 3-4 samples derive.

This suggests more localized redistribution of volatile elements in ordinary chondrites and only limited transmission throughout the parent body.

Fehr et al. (2018) observed large Te isotope fractionation among unequilibrated ordinary chondrites, which they attributed to inherited nebular heterogeneities among the components of these samples. These authors further argued that the initial heterogeneities were subsequently homogenized during thermal metamorphism, and that ordinary chondrites of higher petrologic types would be most representative for the isotopic composition of their respective parent bodies. However, the data of this study reveal variable $\delta^{128/126}$Te among equilibrated ordinary chondrites, indicating either that Te isotopes were not homogenized or, as argued above, were subsequently generated during thermal metamorphism. Either way, the bulk $\delta^{128/126}$Te of ordinary chondrite parent bodies remains relatively imprecisely defined and likely falls in the range between –0.11 (Zhovtnevyi H6) and 0.23 (Aumale L6).

4.3 Tellurium stable isotope composition of bulk silicate Earth

Fehr et al. (2018) reported Te isotope variations of ~0.18‰ amu^{-1} among a variety of terrestrial sediments and geological reference samples and argued that the Te isotopic composition of BSE likely falls within this range. The samples analyzed by Fehr et al. (2018) were mainly chosen because of their high Te abundances, but since these samples likely record Te isotope fractionation during various geological processes, they may not represent the BSE's Te isotope composition. Instead, the chemical composition of the BSE is often inferred based on fertile lherzolites (e.g., Palme and O'Neill, 2014) and such samples may, therefore, be more suitable for constraining the BSE's Te isotope composition. For instance, Wang and Becker (2013) used fertile lherzolites to infer the concentrations of S, Se, and Te in the BSE, and some of the samples used by these authors were also analyzed in the present study.

One problem for estimating the BSE's composition using lherzolites is that their compositions have been modified by the reactive infiltration of primitive basic melt into previously melt-depleted peridotite. This "refertilization" replenishes the inventory of incompatible elements through precipitation of clinopyroxene, Al-phases, and sulfides (e.g., Bodinier and Godard, 2014; Le Roux et al., 2007). The accuracy with which the BSE composition can be reconstructed based on the composition of fertile lherzolites, therefore, depends on how well the melt extraction and subsequent refertilization history of fertile mantle lherzolites can be reconstructed. Wang and Becker (2013;2015a) argued that refertilization is a consequence of the recycling of moderately incompatible elements (e.g., Al, Ca, HREE, but also Re, S, Se and Te), which are ultimately sourced from subducted oceanic crust. These authors further argued that such mixing and re-homogenization processes in the mantle lead to correlations between elements of similar incompatibility (e.g., Al-S-Se-Te, Wang and Becker, 2013), and that, therefore, the minor variations of S-Se-Te ratios among mantle lherzolites should allow precise and accurate estimates of BSE abundances and element ratios. However, others have argued that the Se-Te systematics of fertile lherzolites reflect complex mixing and fractionation processes during refertilization and the precipitation of sulfides from silicate melt, and therefore, do not provide a firm constraint on the Se and Te abundances of the BSE (e.g., König et al., 2014; Lorand and Alard, 2010; Luguet et al., 2015; Yierpan et al., 2019). To this end, Yierpan et al. (2019) argued that for elements like Se and Te, the BSE abundances may also be estimated using the composition of mid-ocean ridge basalts (MORBs) combined with a petrogenetic model for the fractionation of Se and Te during partial melting. On this basis, these authors found that the Se-Te systematics of MORBs are best accounted

for by a source composition having lower Se and Te abundances and a higher Se/Te ratio (49±11 ng g^{-1} Se; 3.5±1.3 ng g^{-1} Te) than estimated from fertile lherzolites (80±17 ng g^{-1} Se; 11.0±1.7 ng g^{-1} Te) (Wang and Becker, 2013). The disparate results of these approaches highlight that current estimates of the BSE's Se and Te abundances are somewhat uncertain.

The Te isotopic data for peridotites from this study may help to shed further light on this issue and, ultimately, to estimate the $\delta^{128/126}$Te value of the BSE. The investigated peridotites are some of the same samples previously used by Wang and Becker (2013) to estimate the BSE's Te concentration. These samples have Al_2O_3 contents ranging from 0.3 to 4.3 wt.%, indicating melt extraction and variable degrees of refertilization (Wang and Becker, 2013). The lherzolites with Al_2O_3 contents of ≥2.8 wt.% exhibit indistinguishable $\delta^{128/126}$Te values averaging at 0.09±0.03 (±2s.d.) and show a narrow range of Te concentrations averaging at 10.7±1.8 ng g^{-1} Te (±2s.d.) (Fig. 7). The nine lherzolites have slightly lower Al_2O_3 contents than current BSE estimates (4.5±0.4 wt.% Al_2O_3; Palme and O'Neill, 2014), but these samples neither show significant $\delta^{128/126}$Te variations nor are they different from the range of Te concentrations of other fertile lherzolites or the BSE estimate of 11.0±1.7 ng g^{-1} (Wang and Becker, 2013). In contrast, the peridotites having Al_2O_3 contents of <2.8 wt.% vary in $\delta^{128/126}$Te between 0.00±0.01 (BM-11-11) and 0.11±0.01 (BD 92-2) and have variable Te concentrations between 2.9 and 8.1 ng g^{-1}, lower than those of the fertile lherzolites (Fig. 7). There is no direct correlation between $\delta^{128/126}$Te and Te concentration (Fig. 3a), although the $\delta^{128/126}$Te of these samples are generally similar to or slightly lighter than the Te isotope composition of the fertile lherzolites. The lower $\delta^{128/126}$Te values may reflect Te isotope fractionation during partial melting or variable degrees of refertilization. If correct, the highly variable degrees of partial melting and refertilization among the analyzed peridotites suggest only minor Te isotope fractionation during these processes (~0.05 ‰ amu^{-1}) (Fig. 7). In this case, Te isotope fractionation during partial melting was limited and isotopic differences between harzburgites and infiltrating melts were small in order to generate the limited range of $\delta^{128/126}$Te between harzburgites and lherzolites. Alternatively, the entire Te budget in the lherzolites derived from an isotopically homogenous source and the Te isotope composition of lherzolites solely represents that of the refertilizing melt.

The two websterites and one orthopyroxenite investigated in this study exhibit similar or slightly heavier $\delta^{128/126}$Te than the lherzolites, but are characterized by more heterogeneous Te concentrations of 13-104 ng g^{-1}, which are higher than those of the lherzolites (Fig. 3). Wang and Becker (2015b) argued that websterites and orthopyroxenites from the Balmuccia massif formed as cumulates from primitive melts that were modified by interaction with peridotitic wall rock, which would be consistent with the limited Te isotope fractionation relative to the peridotite source. By contrast, clinopyroxenites are thought to derive from melts that already have undergone sulfide segregation (Wang and Becker, 2015b). This sulfide segregation may have caused Te extraction from the parent melt, resulting in lower Te concentrations (~2-12 ng g^{-1}) and more variable Te isotopic compositions ($\delta^{128/126}$Te of –0.37 to 0.32) (Fig. 3). This isotopic variability may have been induced by isotope fractionation between sulfide and silicate melts, similar to variations of Cu isotopes in the pyroxenites (Zou et al., 2019). Due to their major element composition and magmatic origin, pyroxenites are unsuitable for constraining the Te isotope composition of BSE.

Thus, the only ultramafic mantle rocks that can potentially provide a reliable estimate for the BSE's Te isotope composition are lherzolites. However, as noted above, owing to the melt depletion and refertilization history of these rocks, it remains controversial if these rocks are suitable to constrain the Te abundance and isotopic composition of the BSE. For instance, König et al. (2014) argued that the Te budget of fertile lherzolites can be modelled by mixing residual monosulfide solid solutions (and platinum group

minerals) with presumed metasomatic low-temperature phases. If correct, fertile lherzolites are unlikely to provide stringent constraints on the composition of the BSE. However, the clinopyroxenites analyzed in this study suggest that sulfide segregation is associated with significant Te isotope fractionation, and so mixing between different sulfide phases during refertilization may result in variable Te isotope compositions. The limited Te isotopic variation among the lherzolites may, therefore, be interpreted to indicate that combined partial melting, refertilization, and metasomatism did not significantly modify the original Te isotope composition. In this case the mean $\delta^{128/126}$Te of 0.09±0.03 ‰ (2.s.d) of the lherzolites may provide a good estimate of the BSE's Te isotopic composition. However, it is also possible that the limited Te isotope variations among the lherzolites merely reflect homogenization during refertilization or a homogeneous $\delta^{128/126}$Te of the refertilizing melt. In these cases, it remains unclear whether the lherzolites represent the $\delta^{128/126}$Te of the BSE. Distinguishing between these possibilities, and better constraining the BSE's $\delta^{128/126}$Te in the process, will require a better understanding of Te isotope fractionation during partial melting and an assessment of the Te isotope composition of the depleted mantle. However, for the time being, we will use the mean $\delta^{128/126}$Te = 0.09±0.03 ‰ (2.s.d) of the lherzolites as the current best estimate for the BSE's Te isotopic composition, with the caveat that this value may change with new results of future studies.

4.4 Comparison between BSE and chondrites and implications for the late veneer

The abundances of S, Se, and Te in the BSE are commonly assumed to have been established predominantly by the late veneer (e.g., Palme and O'Neill, 2014; Wang and Becker, 2013). This notion is based on the observation that these three elements seem to occur in broadly chondritic relative abundances in the BSE and display stronger depletions than the HSE, which entirely derive from the late veneer. Moreover, metal-silicate partitioning experiments suggest that Te is highly siderophile during core formation (Rose-Weston et al., 2009), such that all pre-late veneer Te should have been removed to the core. If correct, then the Te isotope composition of the BSE should reflect that of the late veneer. Thus, comparison of the Te isotope compositions of chondrites and the BSE may help assessing the origin and nature of the late veneer.

Among the carbonaceous chondrites, the BSE's Te isotopic composition ($\delta^{128/126}$Te = 0.09±0.03) overlaps with those of CM chondrites ($\delta^{128/126}$Te = 0.08±0.02; n = 6) and Tagish Lake ($\delta^{128/126}$Te = 0.11±0.01), whereas CV, CO, and CR chondrites show significantly lighter, and CI chondrites slightly heavier $\delta^{128/126}$Te compared to the BSE (Figs. 1,8). This is consistent with the observation that only material similar to CM chondrites and Tagish Lake fit the coupled Se/Ir and Te/Ir systematics of the BSE as inferred from fertile lherzolites (Wang and Becker, 2013). Although it is tempting to interpret this consistent link between the Se-Te elemental and Te isotopic systematics of CM chondrites and the BSE as inferred from fertile lherzolites as evidence for a CM-like source of the late veneer, it is important to recognize that the BSE's $\delta^{128/126}$Te also overlaps with those of enstatite chondrites (and also falls within the range of ordinary chondrites). As noted above, the Te isotopic compositions of type 3-4 EL and EH chondrites were likely modified by addition of isotopically light Te during parent body thermal metamorphism, such that the bulk $\delta^{128/126}$Te of enstatite chondrite parent bodies is likely be heavier than the value measured for type 3-4 enstatite chondrites. Although it remains difficult to quantify this effect, it seems likely that this bulk $\delta^{128/126}$Te overlaps with the BSE value, given that the $\delta^{128/126}$Te of type 3-4 enstatite chondrites is only slightly below that

of the BSE (Fig. 8). Thus, the Te isotopic composition of the BSE alone is equally consistent with an enstatite chondrite-like and CM chondrite-like late veneer. As such, the former could only be excluded based on the higher Se/Te ratios of ~12–13 of enstatite chondrites (Wang and Lipschutz, 2005) compared to the BSE's Se/Te of 8±2 as inferred from fertile lherzolites (Wang and Becker, 2013). However, as noted above, Yierpan et al. (2019) inferred a higher Se/Te ratio of ~14 for the BSE, which essentially is the ratio of enstatite chondrites. Thus, given current estimates, the Te isotopic and Se-Te elemental systematics are equally consistent with a CM-like and enstatite chondrite-like late veneer.

Additional constraints on the nature of the late veneer may be obtained by also considering Se isotope variations. As for Te, the BSE's Se may predominantly derive from the late veneer and may then be used to constrain its origin in a similar manner as Te. Again, the Se isotope composition of peridotites overlaps with CM (and CI) chondrites (Varas-Reus et al., 2019), but, as for Te, this composition likely was modified during the partial melting and refertilization history of these peridotites, and so it remains unclear how well these samples reflect the Se isotopic composition of the BSE. Of note, Yierpan et al. (2019) argued that there is no significant Se isotope fractionation between sulfide and silicate melts during MORB petrogenesis and that, therefore, MORBs preserve the Se isotopic signature of their mantle source, which may in turn reflect the composition of the BSE. This composition is somewhat lighter than the composition of the peridotites, overlaps with the Se isotopic composition of ordinary chondrites, and is only slightly heavier that the composition of enstatite chondrites (Labidi et al., 2018; Vollstaedt et al., 2016). Thus, as for Te, the interpretation of the Se isotopic data with regard to constraining late accretionary sources heavily hinges on how well peridotites represent the composition of the BSE. Moreover, only a limited number of enstatite chondrites have so far been analyzed for Se isotopes and although they all agree within measurement uncertainty, it is unclear as to whether these compositions were modified during parent body metamorphism in a similar manner as observed for other volatile elements like Zn, Te, and Cd (see above). Thus, although terrestrial peridotites and CI chondrites display remarkably similar Se isotope compositions, the fidelity of this observation for constraining the source of the late veneer is unclear.

The interpretation of the Te and Se isotopic data is further complicated by the possibility that not all the Se and Te in the BSE derives from the late veneer. For instance, Labidi et al. (2013) argued that the BSE's S isotopic composition is isotopically fractionated due to core formation, which would require that not all of the S in the BSE derives from late accretion. By contrast, experimental results of Rose-Weston et al. (2009) suggest that S, Se, and Te were all strongly siderophile during core formation and that metal segregation should have induced strong S-Se-Te fractionations. These authors, therefore, argued that the S-Se-Te abundances in the BSE are best explained by late accretion. However, the metal-silicate partitioning experiments of Rose-Weston et al. (2009) were performed at pressures of less than ~20 GPa, requiring large extrapolation to the appropriate conditions for formation of Earth's core at estimated pressures of up to 45-65 GPa (e.g., Rubie et al., 2011). To this end, more recent experimental work within this pressure range reveals that S becomes less siderophile and, therefore, may not be quantitatively removed into Earth's core (Boujibar et al., 2014; Suer et al., 2017). It is unknown at present if the metal-silicate partitioning of Se and Te changes in a similar manner, and so it cannot be excluded that some of the BSE's Se and Te does not derive from the late veneer. Although the near-chondritic relative abundances of S, Se, and Te in the BSE seem to argue against significant fractionation of these elements due to core formation (Wang and Becker, 2013), it is important to recognize that there is substantial variations in S-Se-Te ratios among chondrites (e.g., Se/Te ~8 to ~13; and considerably higher for some metamorphosed samples). Thus, while the S-Se-Te elemental systematics of the BSE falls within the range of chondritic values, this

does not preclude some fractionation of these elements during core formation, which then may have been overprinted to some extent by addition of the late veneer. As such, some of the BSE's Se and Te may be inherited from before late accretion and may, therefore, be isotopically distinct, either because it derives from a different source or because metal-silicate-sulfide partitioning during core formation induced some isotope fractionation (Labidi and Cartigny, 2016; Labidi et al., 2013). Addressing this issue will require a better understanding of the metal-silicate partitioning of Se and Te under relevant core formation conditions, and an assessment of whether core formation can induce significant Se or Te isotope fractionation. Given the high temperatures of core formation, any such isotope fractionation is likely very small, but, as shown above, even a small shift in the isotopic composition may have a significant effect on the interpretation of Se and Te isotope signatures with regard to the source of the late veneer.

Overall, due to uncertainties in the composition of the BSE, and whether or not fertile lherzolites provide a good estimate for that composition, we find that neither a carbonaceous chondrite-like nor an enstatite chondrite-like late veneer can be ruled out from the Se-Te elemental and isotopic systematics alone. This problem is exacerbated by the possibility that not all the BSE's Se and Te may derive from the late veneer, and also by elemental and isotopic fractionation of these elements on some chondrite parent bodies, which renders it difficult to determine their bulk Se-Te elemental and isotopic compositions. In general terms, the results of this study highlight that elemental ratios and mass-dependent isotope compositions are modified by physical and chemical processes occurring after planetary accretion, which makes identifying the original source signatures inherently uncertain and severely limits the use of elemental ratios and mass-dependent isotope fractionations as genetic tracers.

5 Conclusions

This study, combined with data from a companion study (Hellmann et al., 2020), comprises the largest set of Te isotopic data for bulk chondrites that is currently available. Carbonaceous chondrites display homogeneous within-group Te isotope compositions, which systematically vary with the mass fraction of matrix in each group. The Te isotope variations among carbonaceous chondrites, therefore, result from mixing between isotopically light, volatile-depleted chondrules/chondrule precursors and isotopically heavy, volatile-rich CI-like matrix (Hellmann et al., 2020). By contrast, enstatite, ordinary, and Rumuruti chondrites display large within-group Te isotope variations. These are best explained by volatilization and redistribution of Te during thermal metamorphism on the chondrite parent bodies. For enstatite chondrites, the data of this study show increasingly heavy Te isotopic compositions and decreasing Te concentrations with increasing degree of metamorphism, indicating migration of isotopically light Te from the strongly metamorphosed inner parts towards the cooler outer regions of the parent bodies. Of note, the type 3-4 enstatite chondrites of this study have rather uniform $\delta^{128/126}$Te values, suggesting that the added Te from deeper parts of the parent bodies was efficiently homogenized during metamorphism, or alternatively that type 3-4 and 5-6 samples derive from separate bodies. By contrast, ordinary and Rumuruti chondrites display less systematic Te isotope variations, implying more localized redistribution of Te during thermal metamorphism on the parent bodies.

This study also provides the first mass-dependent Te isotope data for terrestrial peridotites. The mantle lherzolites of this study have rather homogeneous Te isotopic compositions, and are used to estimate the $\delta^{128/126}$Te of the BSE. This value overlaps with the $\delta^{128/126}$Te of some volatile-rich carbonaceous

chondrites (most notably CM chondrites), but also with the inferred bulk $\delta^{128/126}$Te of enstatite chondrites and the imprecisely defined $\delta^{128/126}$Te of ordinary chondrites. When the Te isotopic data are considered together with Se isotopic data and S-Se-Te ratios, then the composition of the BSE as inferred from terrestrial peridotites overlaps only with the composition of CM chondrites. Although it is tempting to interpret this observation as evidence for a carbonaceous chondrite-like source of the late veneer, this conclusion heavily depends on how well the peridotites reflect the BSE's composition. If instead the Te isotope data of this study are combined with the BSE's Se/Te ratio and Se isotopic composition as inferred for the mantle source of MORBs (Yierpan et al., 2019), then all data would allow for an enstatite chondrite-like late veneer. Further complications arise if not all the BSE's Se and Te derive from the late veneer, and because elemental and isotopic fractionations during thermal metamorphism make determining bulk compositions of chondrite parent bodies uncertain. Combined, these observations demonstrate that at present neither a carbonaceous chondrite-like nor an enstatite chondrite-like late veneer can be ruled out from the Se-Te elemental and isotopic systematics alone.

The results of this study highlight that the relative abundances and mass-dependent isotope compositions of volatile elements like Se and Te are substantially modified by physical and chemical processes occurring after planetary accretion, which hampers the use of these elements as genetic tracers. By contrast, nucleosynthetic isotope anomalies are not significantly affected by post accretionary processes and, as such, provide the most direct constraints on genetic relationships among different planetary building blocks. To this end, prior studies based on nucleosynthetic Ru isotope anomalies have shown that the late veneer most likely derives from inner solar system material with an on average enstatite chondrite-like isotopic composition (Bermingham and Walker, 2017; Fischer-Gödde and Kleine, 2017; Hopp et al., 2020). Moreover, the isotopic similarity with enstatite chondrites extends to Earth's main building material for a range of geochemically distinct elements that record different stages of Earth's accretion (Dauphas, 2017). The most straightforward interpretation of this persistent isotopic link is that Earth predominantly accreted from inner solar system material throughout its accretion history and including the late veneer, consistent with the idea that the late veneer predominantly derives from the left-over planetesimal population that remained in the terrestrial planet region after the last giant impact on Earth (e.g., Jacobson et al., 2014). Our finding that the Se-Te systematics are not inconsistent with an enstatite chondrite-like late veneer supports this model.

Acknowledgements

We gratefully acknowledge NASA, the Max Planck Institute for Chemistry, Mainz, the US Museum of Natural History, the Field Museum Chicago, the Natural History Museum, London, and the Naturhistorisches Museum Wien for providing meteorite specimens. Antarctic meteorite samples are recovered by the Antarctic Search for Meteorites (ANSMET) program which has been funded by NSF and NASA, and characterized and curated by the Department of Mineral Sciences of the Smithsonian Institution and Astromaterials Curation Office at NASA Johnson Space Center. We thank Manuela Fehr for providing aliquots of Te standard solutions used in prior studies. Constructive reviews by three anonymous reviewers, and the editorial efforts of L. Qin are gratefully acknowledged. Funded by the Deutsche Forschungsgemeinschaft (DFG, German Research Foundation) – Project-ID 263649064 – TRR 170. This is TRR170 publication No. 114.

References

Becker H., Horan M., Walker R., Gao S., Lorand J.-P., Rudnick R. (2006) Highly siderophile element composition of the Earth's primitive upper mantle: constraints from new data on peridotite massifs and xenoliths. *Geochimica et Cosmochimica Acta* **70**, 4528-4550.

Bermingham K., Walker R. (2017) The ruthenium isotopic composition of the oceanic mantle. *Earth and planetary science letters* **474**, 466-473.

Bermingham K., Worsham E., Walker R. (2018) New insights into Mo and Ru isotope variation in the nebula and terrestrial planet accretionary genetics. *Earth and Planetary Science Letters* **487**, 221-229.

Bodinier J., Godard M. (2014) Orogenic, Ophiolitic, and Abyssal Peridotites, in: Carlson R. W. (Ed.), Treatise on Geochemistry, 2 ed. Elsevier, Oxford, pp. 103-167.

Boujibar A., Andrault D., Bouhifd M. A., Bolfan-Casanova N., Devidal J.-L., Trcera N. (2014) Metal–silicate partitioning of sulphur, new experimental and thermodynamic constraints on planetary accretion. *Earth and Planetary Science Letters* **391**, 42-54.

Chou C.-L. (1978) Fractionation of siderophile elements in the Earth's upper mantle. *Lunar and Planetary Science Conference Proceedings*, pp. 219-230.

Dauphas N. (2017) The isotopic nature of the Earth's accreting material through time. *Nature* **541**, 521-524.

Dauphas N., Davis A. M., Marty B., Reisberg L. (2004) The cosmic molybdenum–ruthenium isotope correlation. *Earth and Planetary Science Letters* **226**, 465-475.

Day J. M., Walker R. J., Warren J. M. (2017) 186Os–187Os and highly siderophile element abundance systematics of the mantle revealed by abyssal peridotites and Os-rich alloys. *Geochimica et Cosmochimica Acta* **200**, 232-254.

Fehr M. A., Hammond S. J., Parkinson I. J. (2018) Tellurium stable isotope fractionation in chondritic meteorites and some terrestrial samples. *Geochimica et Cosmochimica Acta* **222**, 17-33.

Fischer-Gödde M., Becker H. (2012) Osmium isotope and highly siderophile element constraints on ages and nature of meteoritic components in ancient lunar impact rocks. *Geochimica et Cosmochimica Acta* **77**, 135-156.

Fischer-Gödde M., Becker H., Wombacher F. (2011) Rhodium, gold and other highly siderophile elements in orogenic peridotites and peridotite xenoliths. *Chemical Geology* **280**, 365-383.

Fischer-Gödde M., Burkhardt C., Kruijer T. S., Kleine T. (2015) Ru isotope heterogeneity in the solar protoplanetary disk. *Geochimica et Cosmochimica Acta* **168**, 151-171.

Fischer-Gödde M., Elfers B.-M., Münker C., Szilas K., Maier W. D., Messling N., Morishita T., Van Kranendonk M., Smithies H. (2020) Ruthenium isotope vestige of Earth's pre-late-veneer mantle preserved in Archaean rocks. *Nature* **579**, 240-244.

Fischer-Gödde M., Kleine T. (2017) Ruthenium isotopic evidence for an inner Solar System origin of the late veneer. *Nature* **541**, 525-527.

Friedrich J. M., Bridges J. C., Wang M.-S., Lipschutz M. E. (2004) Chemical studies of L chondrites. VI: Variations with petrographic type and shock-loading among equilibrated falls. *Geochimica et Cosmochimica Acta* **68**, 2889-2904.

Hellmann J. L., Hopp T., Burkhardt C., Kleine T. (2020) Origin of volatile element depletion among carbonaceous chondrites. *Earth and Planetary Science Letters* **549**, 116508.

Hopp T., Budde G., Kleine T. (2020) Heterogeneous accretion of Earth inferred from Mo-Ru isotope systematics. *Earth and Planetary Science Letters* **534**, 116065.

Hopp T., Kleine T. (2018) Nature of late accretion to Earth inferred from mass-dependent Ru isotopic compositions of chondrites and mantle peridotites. *Earth and Planetary Science Letters* **494**, 50-59.

Ikramuddin M., Binz C., Lipschutz M. (1976) Thermal metamorphism of primitive meteorites—II. Ten trace elements in Abee enstatite chondrite heated at 400–1000° C. *Geochimica et Cosmochimica Acta* **40**, 133-142.

Jacobson S. A., Morbidelli A., Raymond S. N., O'Brien D. P., Walsh K. J., Rubie D. C. (2014) Highly siderophile elements in Earth's mantle as a clock for the Moon-forming impact. *Nature* **508**, 84-87.

Kadlag Y., Becker H. (2017) Origin of highly siderophile and chalcogen element fractionations in the components of unequilibrated H and LL chondrites. *Chemie der Erde-Geochemistry* **77**, 105-119.

Kimura K., Lewis R. S., Anders E. (1974) Distribution of gold and rhenium between nickel-iron and silicate melts: implications for the abundance of siderophile elements on the Earth and Moon. *Geochimica et Cosmochimica Acta* **38**, 683-701.

König S., Lorand J.-P., Luguet A., Pearson D. G. (2014) A non-primitive origin of near-chondritic S–Se–Te ratios in mantle peridotites; implications for the Earth's late accretionary history. *Earth and Planetary Science Letters* **385**, 110-121.

Labidi J., Cartigny P. (2016) Negligible sulfur isotope fractionation during partial melting: Evidence from Garrett transform fault basalts, implications for the late-veneer and the hadean matte. *Earth and Planetary Science Letters* **451**, 196-207.

Labidi J., Cartigny P., Moreira M. (2013) Non-chondritic sulphur isotope composition of the terrestrial mantle. *Nature* **501**, 208-211.

Labidi J., König S., Kurzawa T., Yierpan A., Schoenberg R. (2018) The selenium isotopic variations in chondrites are mass-dependent; Implications for sulfide formation in the early solar system. *Earth and Planetary Science Letters* **481**, 212-222.

Le Roux V., Bodinier J.-L., Tommasi A., Alard O., Dautria J.-M., Vauchez A., Riches A. (2007) The Lherz spinel lherzolite: refertilized rather than pristine mantle. *Earth and Planetary Science Letters* **259**, 599-612.

Lorand J.-P., Alard O. (2010) Determination of selenium and tellurium concentrations in Pyrenean peridotites (Ariege, France): new insight into S/Se/Te systematics of the upper in mantle samples. *Chemical Geology* **278**, 120-130.

Luck J.-M., Othman D. B., Albarède F. (2005) Zn and Cu isotopic variations in chondrites and iron meteorites: early solar nebula reservoirs and parent-body processes. *Geochimica et Cosmochimica Acta* **69**, 5351-5363.

Luguet A., Behrens M., Pearson D. G., König S., Herwartz D. (2015) Significance of the whole rock Re–Os ages in cryptically and modally metasomatised cratonic peridotites: Constraints from HSE–Se–Te systematics. *Geochimica et Cosmochimica Acta* **164**, 441-463.

Mann U., Frost D. J., Rubie D. C., Becker H., Audétat A. (2012) Partitioning of Ru, Rh, Pd, Re, Ir and Pt between liquid metal and silicate at high pressures and high temperatures-Implications for the

origin of highly siderophile element concentrations in the Earth's mantle. *Geochimica et Cosmochimica Acta* **84**, 593-613.

Meisel T., Walker R., Morgan J. (1996) The osmium isotopic composition of the Earth's primitive upper mantle. *Nature* **383**, 517-520.

Meisel T., Walker R. J., Irving A. J., Lorand J.-P. (2001) Osmium isotopic compositions of mantle xenoliths: a global perspective. *Geochimica et Cosmochimica Acta* **65**, 1311-1323.

Moynier F., Paniello R. C., Gounelle M., Albarède F., Beck P., Podosek F., Zanda B. (2011) Nature of volatile depletion and genetic relationships in enstatite chondrites and aubrites inferred from Zn isotopes. *Geochimica et Cosmochimica Acta* **75**, 297-307.

Palme H., O'Neill H. S. C. (2014) Cosmochemical estimates of mantle composition, in: Carlson R. W. (Ed.), Treatise on Geochemistry, 2 ed. Elsevier, Oxford, pp. 1-39.

Richter F. M., Davis A. M., DePaolo D. J., Watson E. B. (2003) Isotope fractionation by chemical diffusion between molten basalt and rhyolite. *Geochimica et Cosmochimica Acta* **67**, 3905-3923.

Rose-Weston L., Brenan J. M., Fei Y., Secco R. A., Frost D. J. (2009) Effect of pressure, temperature, and oxygen fugacity on the metal-silicate partitioning of Te, Se, and S: Implications for earth differentiation. *Geochimica et Cosmochimica Acta* **73**, 4598-4615.

Rubie D. C., Frost D. J., Mann U., Asahara Y., Nimmo F., Tsuno K., Kegler P., Holzheid A., Palme H. (2011) Heterogeneous accretion, composition and core–mantle differentiation of the Earth. *Earth and Planetary Science Letters* **301**, 31-42.

Schaefer L., Fegley B. (2010) Volatile element chemistry during metamorphism of ordinary chondritic material and some of its implications for the composition of asteroids. *Icarus* **205**, 483-496.

Siebert C., Nägler T. F., Kramers J. D. (2001) Determination of molybdenum isotope fractionation by double-spike multicollector inductively coupled plasma mass spectrometry. *Geochemistry, Geophysics, Geosystems* **2**, 2000GC000124.

Suer T.-A., Siebert J., Remusat L., Menguy N., Fiquet G. (2017) A sulfur-poor terrestrial core inferred from metal–silicate partitioning experiments. *Earth and Planetary Science Letters* **469**, 84-97.

Varas-Reus M., König S., Yierpan A., Lorand J.-P., Schoenberg R. (2019) Selenium isotopes as tracers of a late volatile contribution to Earth from the outer Solar System. *Nature Geoscience* **12**, 779-782.

Vollstaedt H., Mezger K., Leya I. (2016) The isotope composition of selenium in chondrites constrains the depletion mechanism of volatile elements in solar system materials. *Earth and planetary science letters* **450**, 372-380.

Walker R. J. (2009) Highly siderophile elements in the Earth, Moon and Mars: update and implications for planetary accretion and differentiation. *Chemie der Erde-Geochemistry* **69**, 101-125.

Walker R. J., Bermingham K., Liu J., Puchtel I. S., Touboul M., Worsham E. A. (2015) In search of late-stage planetary building blocks. *Chemical Geology* **411**, 125-142.

Wang M.-S., Lipschutz M. E. (2005) Thermal metamorphism of primitive meteorites—XII. The enstatite chondrites revisited. *Environmental Chemistry* **2**, 215-226.

Wang Z., Becker H. (2013) Ratios of S, Se and Te in the silicate Earth require a volatile-rich late veneer. *Nature* **499**, 328-331.

Wang Z., Becker H. (2015a) Comment on "A non-primitive origin of near-chondritic S–Se–Te ratios in mantle peridotites: Implications for the Earth's late accretionary history" by König S. et al. [Earth Planet. Sci. Lett. 385 (2014) 110–121]. *Earth and Planetary Science Letters*, 164-166.

Wang Z., Becker H. (2015b) Fractionation of highly siderophile and chalcogen elements during magma transport in the mantle: constraints from pyroxenites of the Balmuccia peridotite massif. *Geochimica et Cosmochimica Acta* **159**, 244-263.

Wang Z., Becker H., Gawronski T. (2013) Partial re-equilibration of highly siderophile elements and the chalcogens in the mantle: A case study on the Baldissero and Balmuccia peridotite massifs (Ivrea Zone, Italian Alps). *Geochimica et Cosmochimica Acta* **108**, 21-44.

Wombacher F., Rehkämper M., Mezger K. (2004) Determination of the mass-dependence of cadmium isotope fractionation during evaporation. *Geochimica et cosmochimica acta* **68**, 2349-2357.

Wombacher F., Rehkämper M., Mezger K., Bischoff A., Münker C. (2008) Cadmium stable isotope cosmochemistry. *Geochimica et Cosmochimica Acta* **72**, 646-667.

Wombacher F., Rehkämper M., Mezger K., Münker C. (2003) Stable isotope compositions of cadmium in geological materials and meteorites determined by multiple-collector ICPMS. *Geochimica et Cosmochimica Acta* **67**, 4639-4654.

Wood B. J., Smythe D. J., Harrison T. (2019) The condensation temperatures of the elements: A reappraisal. *American Mineralogist: Journal of Earth and Planetary Materials* **104**, 844-856.

Worsham E. A., Burkhardt C., Budde G., Fischer-Gödde M., Kruijer T. S., Kleine T. (2019) Distinct evolution of the carbonaceous and non-carbonaceous reservoirs: Insights from Ru, Mo, and W isotopes. *Earth and Planetary Science Letters* **521**, 103-112.

Yamaguchi A., Scott E. R., Keil K. (1999) Origin of a unique impact-melt rock—the L-chondrite Ramsdorf. *Meteoritics & Planetary Science* **34**, 49-59.

Yierpan A., König S., Labidi J., Schoenberg R. (2019) Selenium isotope and S-Se-Te elemental systematics along the Pacific-Antarctic ridge: Role of mantle processes. *Geochimica et Cosmochimica Acta*.

Zou Z., Wang Z., Li M., Becker H., Geng X., Hu Z., Lazarov M. (2019) Copper isotope variations during magmatic migration in the mantle: Insights from mantle pyroxenites in Balmuccia peridotite massif. *Journal of Geophysical Research: Solid Earth* **124**, 11,130-111,149.

Table 1

Tellurium concentrations and isotope data of ordinary, enstatite, and Rumuruti chondrites.

Sample	Classification	Shock	Te (ng/g) (±2σ)	N	$\delta^{128/126}$Te (±2s.d.)
Enstatite chondrites					
Sahara 97072	EH3	S2	1965 ± 48	6	0.16 ± 0.01
GRO 95517	EH3		1744 ± 38	5	0.02 ± 0.04
DOM 14021	EH3		2019 ± 60	5	0.00 ± 0.02
MIL 07028	EH3		2164 ± 71	6	0.00 ± 0.02
LAR 12001	EH3		1928 ± 52	6	-0.03 ± 0.03
LAR 06252	EH3	S4	2008 ± 81	5	-0.04 ± 0.03
EET 87746	EH4	S3	1733 ± 39	6	0.01 ± 0.01
Indarch	EH4	S3	2678 ± 70	4	0.00 ± 0.02
Abee	EH4	S3	2236 ± 38	5	0.00 ± 0.03
St. Mark's	EH5	S3	1265 ± 26	5	0.42 ± 0.03
MAC 02837	EL3	S3	1384 ± 30	5	0.06 ± 0.02
PCA 91020	EL3	S5	1539 ± 56	5	0.02 ± 0.03
MAC 02747	EL4	S4	1479 ± 41	4	0.04 ± 0.02
TIL 91714	EL5	S2	172 ± 19	4	0.48 ± 0.02
Khairpur	EL6	S2	603 ± 31	4	1.56 ± 0.02
LAP 10130	EL6		295 ± 6	5	1.20 ± 0.03
LAR 10014	EL6		325 ± 14	6	0.90 ± 0.03
Pillistfer	EL6	S2	274 ± 6	4	0.70 ± 0.01
Hvittis	EL6	S2	471 ± 15	7	0.60 ± 0.03
LON 94100	EL6	S2	144 ± 4	4	0.56 ± 0.03
ALH 81021	EL6	S2	148 ± 4	4	0.08 ± 0.03
Ordinary chondrites					
Bremervörde	H/L3.9 (H)	S2	494 ± 22	6	-0.29 ± 0.02
Ochansk	H4	S2	402 ± 13	4	-0.10 ± 0.02
Nadiabondi	H5	S2	299 ± 8	5	0.13 ± 0.02
Gao-Guenie	H5	S2	375 ± 13	5	0.21 ± 0.02
Richardton	H5	S2	379 ± 16	5	-0.10 ± 0.02
Kernouve	H6	S1	401 ± 13	4	0.08 ± 0.02
Estacado	H6	S3	437 ± 15	5	-0.01 ± 0.02
Zhovtnevyi	H6	S3	334 ± 10	5	-0.11 ± 0.02
Tennasilm	L4	S2-3	458 ± 31	5	0.23 ± 0.02
Bjurböle	L/LL4 (L)	S1	643 ± 38	3	-0.16 ± 0.04
Ergheo	L5	S4	367 ± 17	8	0.17 ± 0.03
Barwell	L5	S3	400 ± 13	5	0.09 ± 0.02
Knyahinya	L/LL5 (L)	S3	359 ± 14	5	0.87 ± 0.03
Leedey	L6	S3	344 ± 10	5	0.11 ± 0.02
Kunashak	L6	S4	289 ± 10	5	1.48 ± 0.01
Ramsdorf	L6	S4	598 ± 31	8	0.78 ± 0.03
Aumale	L6	S4	325 ± 8	4	0.23 ± 0.04
Parnallee	LL3.6	S3	286 ± 7	5	0.26 ± 0.02
Soko-Banja	LL4	S2	300 ± 8	4	0.12 ± 0.01
Tuxtuac	LL5	S2	262 ± 7	3	0.15 ± 0.02
Rumuruti chondrites					
Almahata Sitta MS-CH	R3.8	S1	756 ± 53	4	0.41 ± 0.01
NWA 753	R3.9		1062 ± 31	6	-0.02 ± 0.03

N = Number of analyses of the same sample digestion

Table 2

Tellurium concentrations and isotope data, Al_2O_3 content, and Se/Te of peridotites and pyroxenites from Balmuccia (BM), Baldissero (BD), Beni Bousera (BB), External Ligurian ophiolite (EL), Turon de Técouère (TUR), and Lanzo (L).

Sample	Rock	Te (ng/g) (±2σ)	N	$\delta^{128/126}$Te (±2s.d.)	Al_2O_3 (wt.%)[a]	Se/Te[a]
Peridotites						
L-72A	L	10.2 ± 0.5	3	0.05 ± 0.02	4.3	
TUR-14	L	10.7 ± 0.6	3	0.10 ± 0.01	4.0	7.4
BB-2C	L	9.5 ± 0.5	3	0.08 ± 0.02	3.9	8.2
BM-9	L	10.8 ± 0.5	5	0.09 ± 0.03	3.4	8.7
EL-1	L	9.5 ± 0.4	3	0.07 ± 0.01	3.4	7.8
BD-11-08	L	10.8 ± 0.4	3	0.08 ± 0.02	3.2	6.6
L-30	L	11.8 ± 0.9	6	0.10 ± 0.04	3.2	
BB-3A	L	10.4 ± 0.5	3	0.11 ± 0.01	3.0	8.5
BM-11-10	L	12.2 ± 0.7	5	0.10 ± 0.04	2.8	7.4
BM-11-11	L	8.1 ± 0.5	3	0.00 ± 0.01	2.1	4.8
BD-92-2	H	6.0 ± 0.4	3	0.11 ± 0.01	1.8	6.6
BM-11-03B	H	7.7 ± 0.6	4	0.06 ± 0.02	1.1	5.5
BM-11-07A	D	2.9 ± 0.1	1	0.04 ± 0.02	0.3	10.1
Pyroxenites						
BM-11-15	Sp-cpx	6.9 ± 0.7	3	-0.37 ± 0.01	11.6	49.8
BM-11-26	Sp-cpx	2.4 ± 0.4	1	0.27 ± 0.02	7.0	
BM-11-28B	Sp-cpx	11.6 ± 0.5	4	0.32 ± 0.02	6.0	40.9
BM-11-07B	Op	104 ± 3	4	0.16 ± 0.02	5.4	5.6
BM-11-19	Web	13.2 ± 0.7	4	0.10 ± 0.01	5.1	16.1
BM-11-21	Web	96 ± 3	4	0.14 ± 0.03	2.7	9.1

[a] Data from Wang and Becker (2013), Wang et al. (2013), Wang and Becker (2015b) and Fischer-Gödde et al. (2011)

N = Number of analyses of the same sample digestion

L: Lherzolite; H: Harzburgite; D: Dunite; Sp-cpx: spinel clinopyroxenite; Op: Orthopyroxenite; Web: Websterite

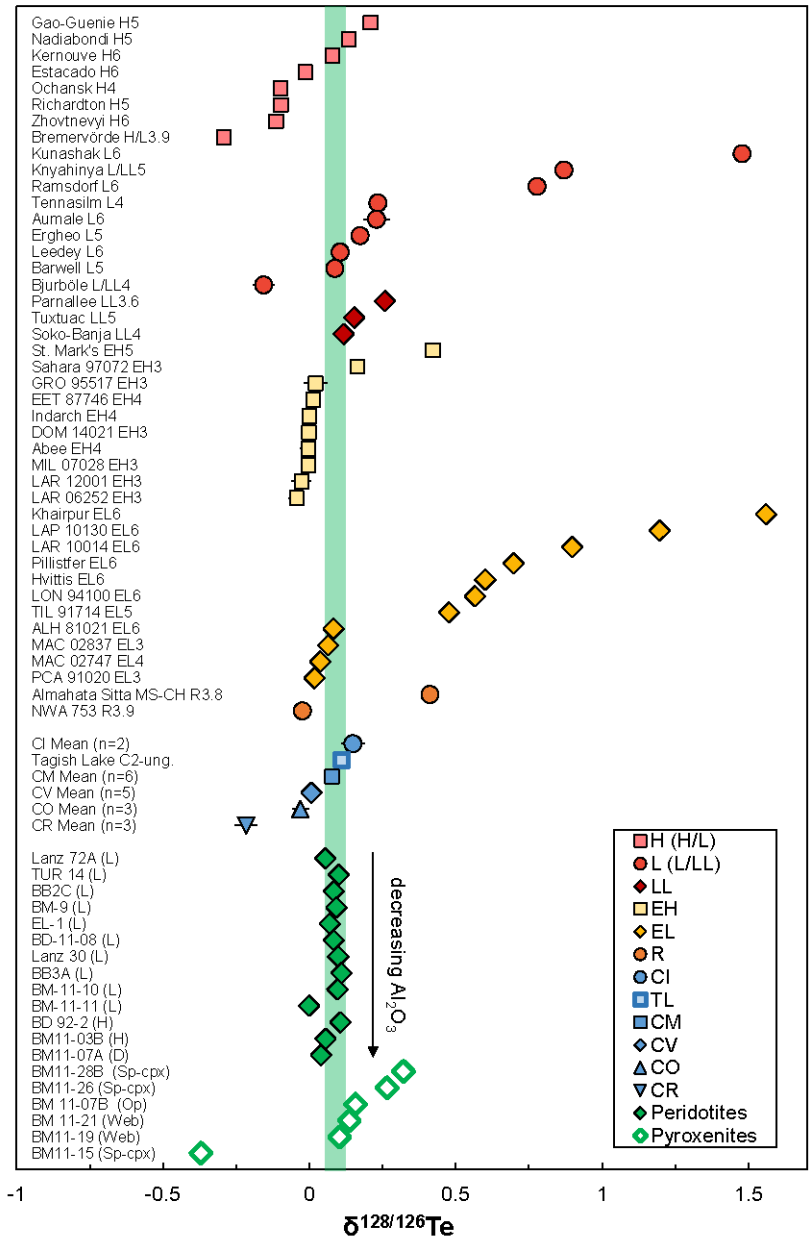

Fig. 1. Tellurium stable isotopic compositions ($\delta^{128/126}$Te relative to SRM 3156) of ordinary (red), enstatite (yellow), Rumuruti (orange), and carbonaceous chondrites (blue) as well as of terrestrial mantle rocks (green). Data for carbonaceous chondrites are from Hellmann et al. (2020). The green bar represents the $\delta^{128/126}$Te inferred for BSE.

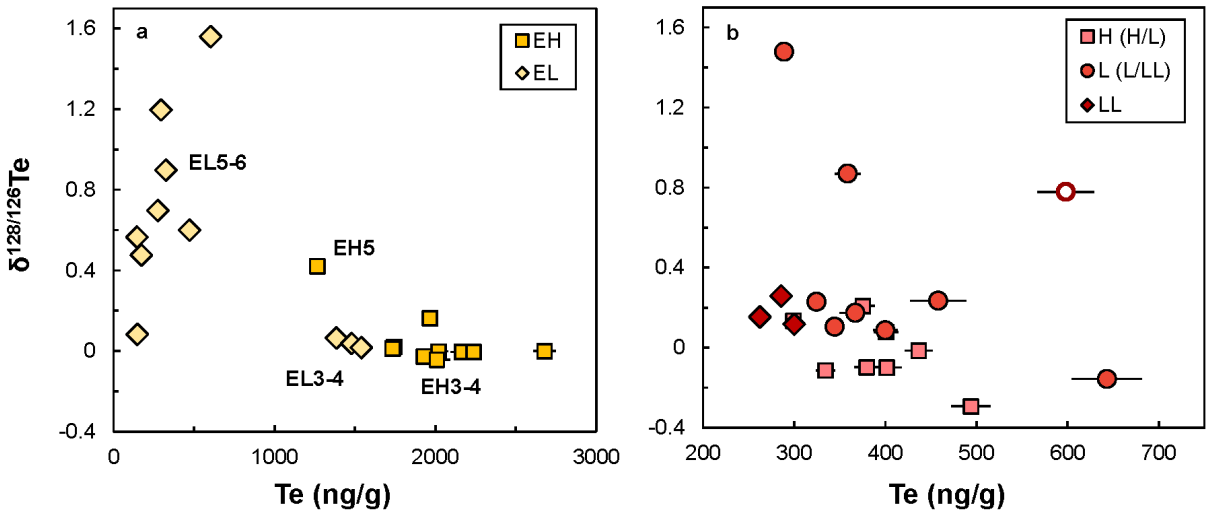

Fig. 2. (**a**) $\delta^{128/126}$Te and Te concentration data for EH and EL chondrites. Type 3-4 samples display high Te concentrations and rather homogeneous $\delta^{128/126}$Te. By contrast, strongly metamorphosed type 5-6 samples are depleted in Te relative to type 3-4 samples and display large variation in $\delta^{128/126}$Te. (**b**) $\delta^{128/126}$Te and Te concentration data for unequilibrated and equilibrated ordinary chondrites of petrologic types 3-6. Open symbol represents the L6 chondrite Ramsdorf, which probably is an impact melt rock (Yamaguchi et al., 1999).

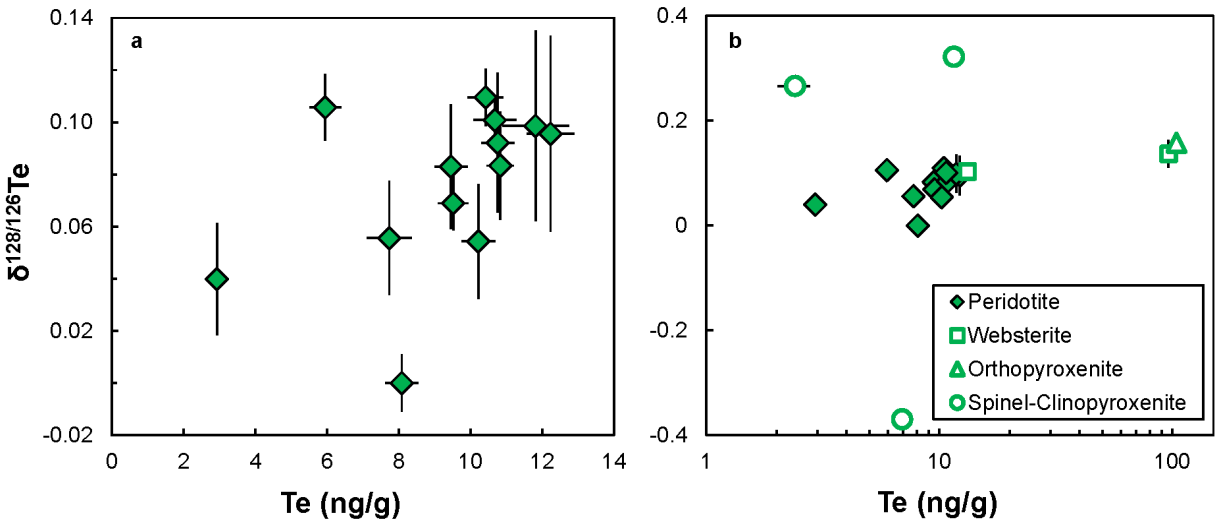

Fig. 3. $\delta^{128/126}$Te and Te concentration data for (**a**) peridotites and (**b**) peridotites and pyroxenites. Closed symbols represent peridotites and open symbols represent pyroxenites. Note that the peridotite data are the same in a) and b), but that the axes have different scales.

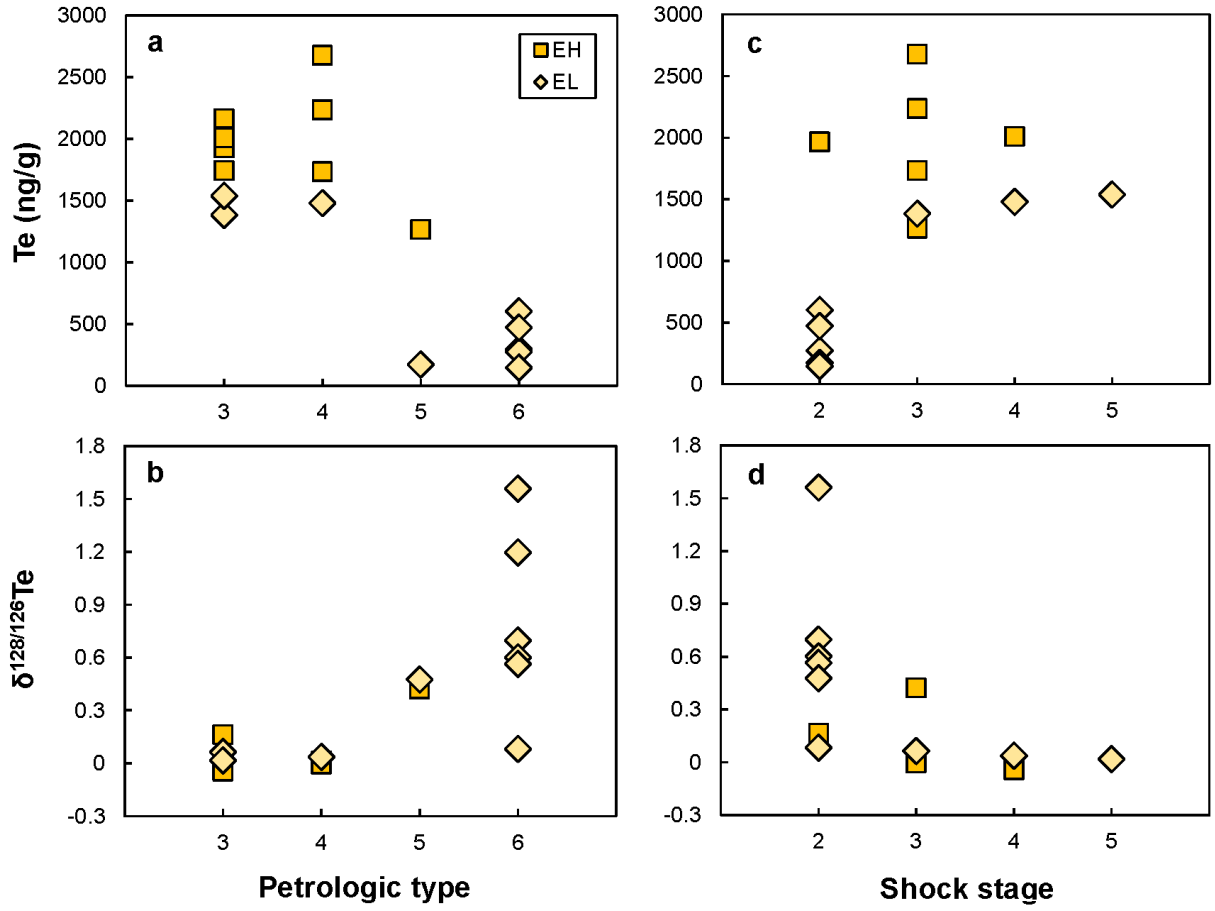

Fig. 4. Tellurium isotopic composition and Te concentration of enstatite chondrites versus petrologic type (**a, b**) and shock stage (**c, d**).

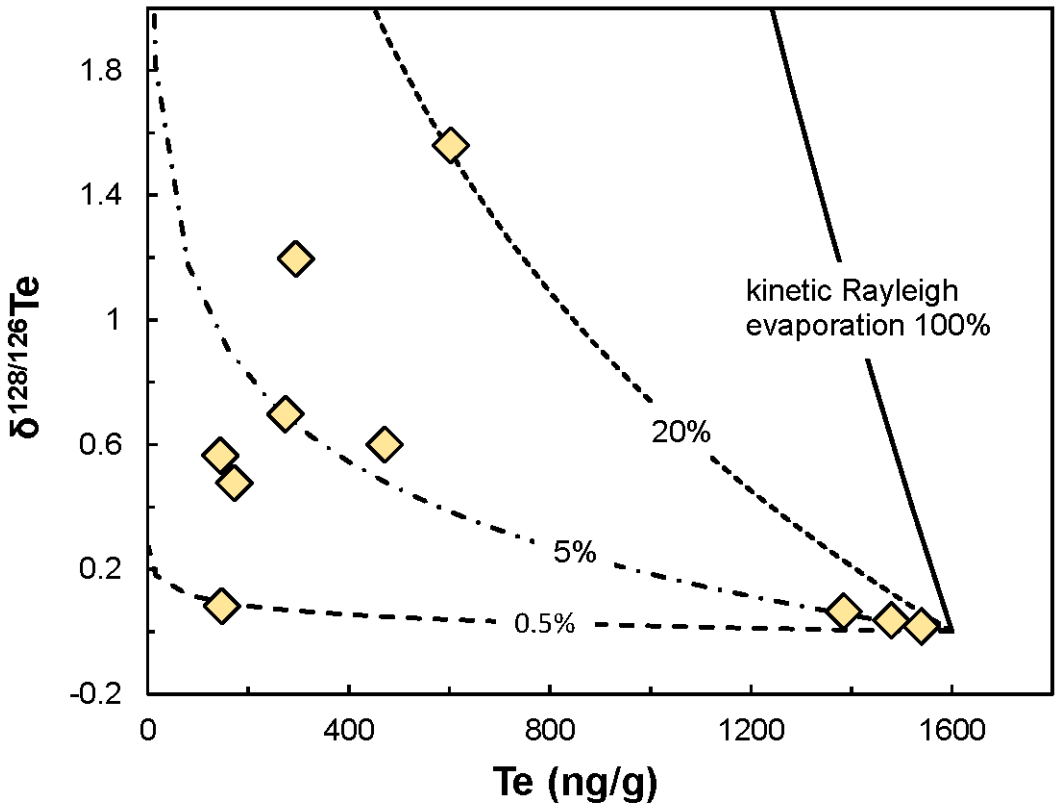

Fig. 5. Relationship of Te depletion and Te isotope fractionation in EL chondrites. Solid line indicates pure kinetic Rayleigh evaporation calculated using a starting composition of $\delta^{128/126}$Te = 0 and [Te] = 1600 ng g^{-1}. The Te isotopic composition of the evaporation residue is given by $\delta^{128/126}\mathrm{Te}_{\mathrm{residue}} = \left(f^{(\alpha_{\mathrm{kin}}-1)} - 1\right) \times 1000$, where f is the mass fraction of Te remaining in the solid and α_{kin} is the kinetic isotope fractionation factor $\alpha_{\mathrm{kin}} = \sqrt{m_{126}/m_{128}}$, where m_{126} and m_{128} are the atomic masses of ^{126}Te and ^{128}Te, respectively. Several studies have shown that kinetic isotope fractionation in experiments and in natural samples typically does not follow the theoretical value of α_{kin}, but that considerably lower values for the isotope fractionation factor are more appropriate (e.g., Richter et al., 2003; Wombacher et al., 2004). Dashed lines indicate kinetic Rayleigh evaporation with variable suppression, showing that the Te isotopic data are consistent with <20% of the fractionation as expected from pure Rayleigh evaporation. This is consistent with prior observation for Cd isotopes in ordinary chondrites (Wombacher et al., 2008).

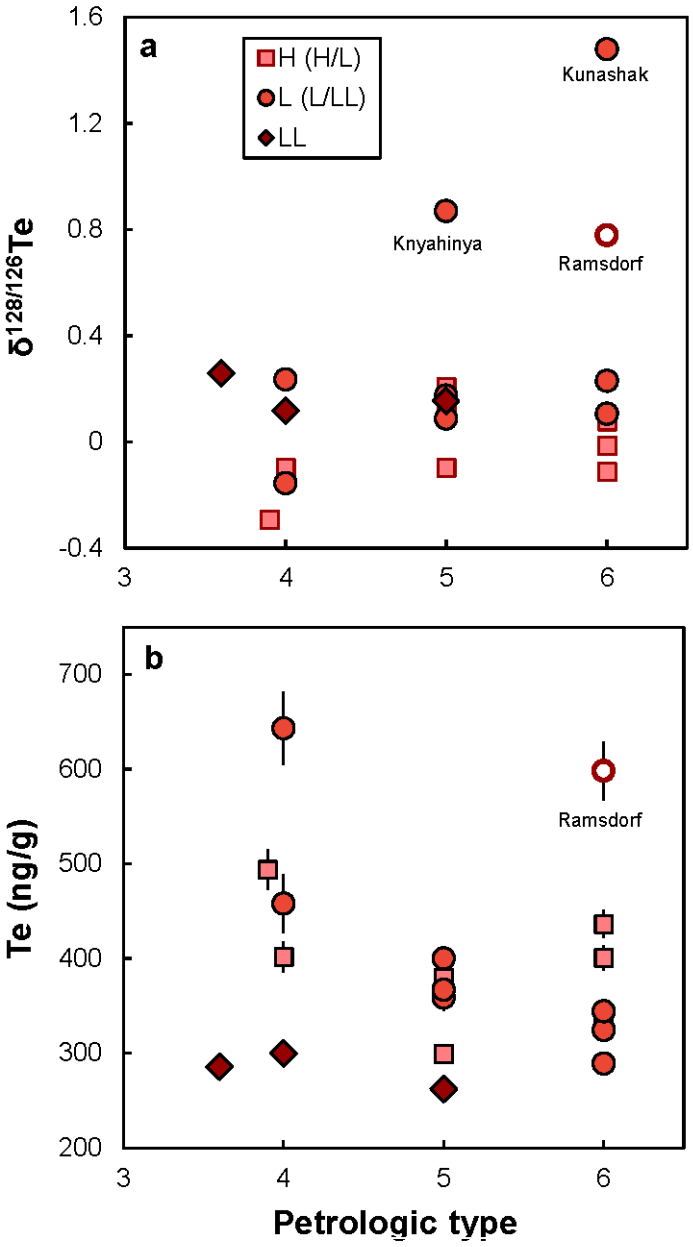

Fig. 6. (**a**) $\delta^{128/126}$Te and (**b**) Te concentration of ordinary chondrites as a function of petrologic type.

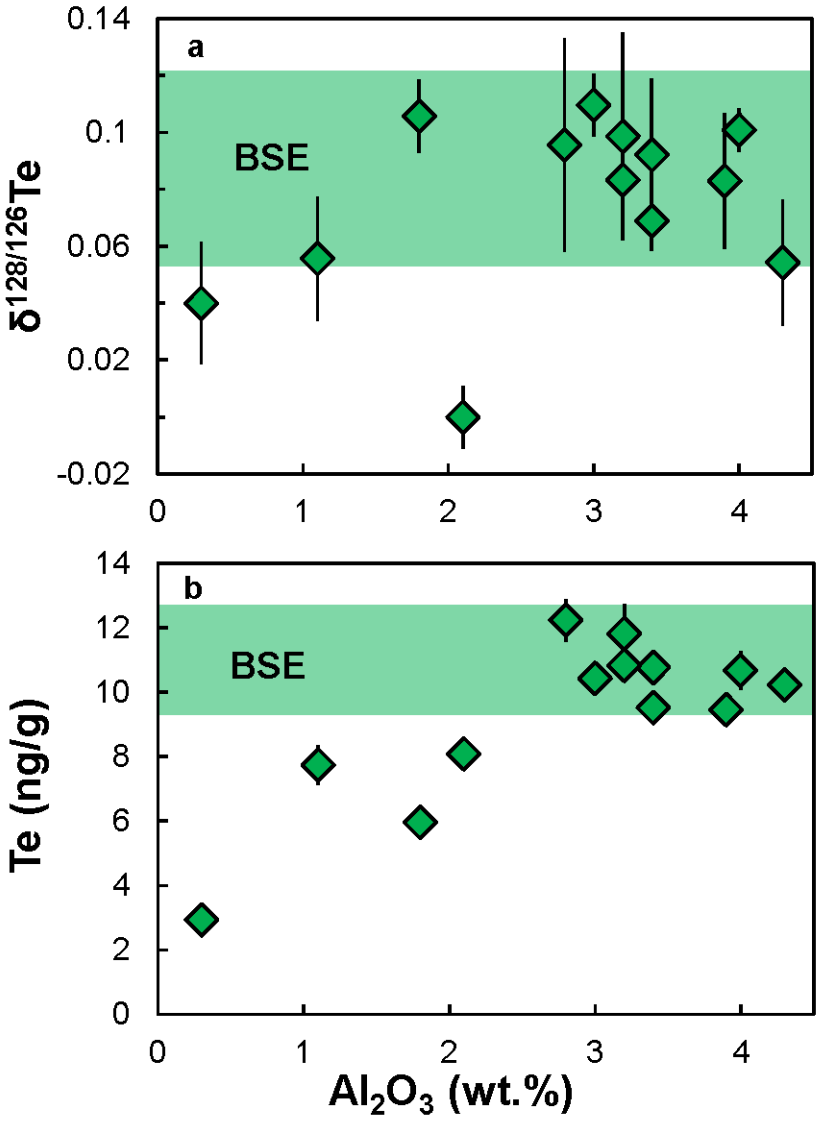

Fig. 7. $\delta^{128/126}$Te (**a**) and Te concentration (**b**) versus Al_2O_3 content of peridotites. Green bars represent the uncertainties (2s.d.) on $\delta^{128/126}$Te and [Te] of fertile lherzolites (Al_2O_3 ≥2.8). Al_2O_3 data are from Wang and Becker (2013), Wang et al. (2013), and Fischer-Gödde et al. (2011).

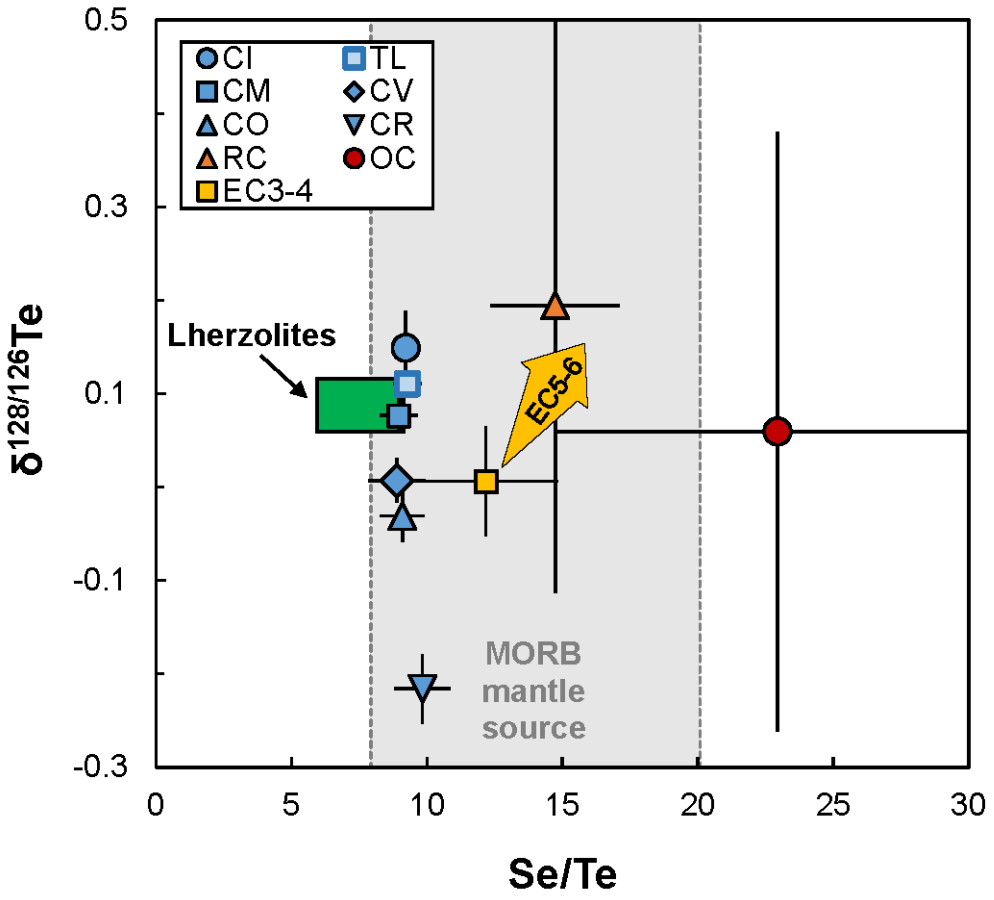

Fig. 8. Mass-dependent Te isotopic compositions of carbonaceous (blue; Hellmann et al., 2020), ordinary (red), enstatite (yellow), and Rumuruti chondrites (orange) compared to Se/Te (for source of Se-Te data see Table S1). TL: Tagish Lake. The green box corresponds to the $\delta^{128/126}$Te and Se/Te inferred for BSE based on lherzolites (this study; Wang and Becker, 2013) and the grey area represents the BSE's Se/Te inferred from MORBs (Yierpan et al., 2019). Note that the $\delta^{128/126}$Te for MORBs is unknown at present.